

Controlling the Large-Scale Motions in a Turbulent Boundary Layer

I. Marusic, K. M. Talluru and N. Hutchins

Abstract In this paper we consider a strategy to manipulate the large-scale structures in wall-bounded turbulent flows, which have recently been shown to be a key mechanism for modulating levels of the skin-friction drag. For this, we use a rectangular wall-normal jet to target the large-scale structures as detected by an upstream spanwise array of skin-friction sensors. A second spanwise array of sensors, located downstream of the jet, records any modifications to the large-scale structure. In addition, a traversing hotwire probe is mounted above the second spanwise array of sensors to study the effects across the depth of boundary layer. It is found that the jet is able to create a low-speed region and when targeted on a high-speed structure changes the associated footprint at the wall.

Keywords Large-scale structures · Skin-friction · Turbulent boundary layer · Wall-normal jet · Flow-control

1 Introduction

Over the past several decades, there has been growing understanding that turbulent boundary layers, despite their obvious randomness, possess certain recurrent features, commonly termed as ‘coherent structures’, and recent studies considerably expanded this view (Adrian 2007). Recent studies of high-Reynolds-number flows in pipe, channel and flat-plate boundary layers have revealed the presence of very large-scale motions (VLSMs, also referred to as superstructures) in the logarithmic regions of turbulent boundary layers, see Kim and Adrian (1999), Tomkins and Adrian (2003) and Hutchins and Marusic (2007a).

I. Marusic (✉) · K. M. Talluru · N. Hutchins
Department of Mechanical Engineering, The University of Melbourne,
Victoria 3010, Australia
e-mail: imarusic@unimelb.edu.au

Hutchins and Marusic (2007b) used a rake of 10 hotwires, and from the time-series data, they reported that these structures extend to large streamwise lengths and substantially meander in the spanwise direction. In addition, they inferred that the larger outer region motions extend down to the wall and modulate the flow in the inner layer, including the buffer layer. Such interactions were quantified by Mathis et al. (2009) and formed the basis of inner–outer motion interaction model by Marusic et al. (2010). Using the model, one could predict the statistics of the streamwise velocity fluctuations in the near-wall region from the large-scale velocity signal in the logarithmic region of a given flow. This idea was further strengthened in other recent studies by Chung and McKeon (2010) and Guala et al. (2011) and Hutchins et al. (2011). They reported methodologies describing how the large-scale features modulate the small-scale fluctuations near the wall. Through conditional average results, Hutchins et al. (2011) observed that associated with the low-skin-friction event, there is reduced small-scale activity near the wall switching to a regime of more intense small-scale fluctuations farther away from the wall.

Using the large-scale shear-stress footprint at the wall, Hutchins et al. (2011) conducted studies using a spanwise array of surface-mounted skin-friction sensors together with a traversing hotwire probe. From such experiments, they obtained a three-dimensional conditionally averaged view of the large-scale superstructures in a turbulent boundary layer. The conditional mean results indicated the presence of a forward-leaning low-speed and high-speed structures above low and high-skin-friction events, respectively, and with anti-correlated regions flanking them.

Many of the studies mentioned above rely only on streamwise velocity information. However, Hutchins and Marusic (2007b) identified counter-rotating roll-like structures associated with the largest scale events using a DNS channel flow database ($Re_\tau = 950$). Dennis and Nickels (2011) computed various conditional averages from high-speed PIV measurements and showed a similar organization in the spanwise vicinity of large-scale structures. Also a study conducted in the atmospheric boundary layer by Hutchins et al. (2012) revealed identical results in the instantaneous velocity vector fields using linear stochastic estimation (LSE) technique.

In a more recent study conducted by Beresh et al. (2011), the focus was switched to wall pressure field from that of velocity field. Interestingly, they observed similar large-scale motions in the wall-pressure fluctuations beneath a supersonic turbulent boundary layer and attributed that such motions are the most possible explanation of the observed low-frequency pressure fluctuations in flight-vehicle vibrations.

In the past, Savill and Mumford (1988) attempted the use of large-eddy break-up (LEBU) devices and reported a significant drag reduction downstream of the LEBUs. They explained it in terms of interactions between the wake from the LEBUs and the large-scale motions in the outer layer of the boundary layer. However, such an approach suffered due to the form drag associated with the devices, diminishing the benefit in the skin-friction drag. Here, we are attempting to eliminate such drawbacks by using a non-intrusive wall-normal jet. Low-Reynolds-number

studies of a jet in cross-flows by Haven and Kurosaka (1997) revealed that a streamwise vortex pair is generated and that the strength of the pair depends on the aspect ratio of the jet. In this investigation, we are using a rectangular jet due to its high-aspect-ratio geometry.

Putting together the wall footprint of the large-scale structures, their modulating effect on the near-wall small-scale fluctuations, their associated streamwise roll modes, and their influence on the pressure fluctuations, it is possible to construct a well-targeted control scheme. With this intent, we are using a wall-normal jet that can generate a roll mode that acts as a retrograde to the naturally occurring roll modes associated with the large-scale structures in a turbulent boundary layer and thereby affect the acoustic noise and turbulence levels across the depth of the boundary layer.

2 Experimental Setup

Experiments were carried out in the high-Reynolds-number boundary layer wind tunnel (HRNBLWT) at the University of Melbourne. This open-return blower wind tunnel has dimensions of $27 \times 2 \times 1$ m with a nominally zero pressure gradient. Further details of the wind tunnel are given in Kulandaivelu (2012). In this current investigation, measurements are conducted in a turbulent boundary layer that has developed over a distance of 21 m from the trip. At a free-stream velocity of 20 m/s, the boundary layer thickness (δ) at the measuring station is 0.326 m. With the friction velocity, $U_\tau = 0.635$ m/s, a Reynolds number close to 14,000 is obtained in these experiments. Here, Reynolds number is defined as $Re_\tau = U_\tau \delta / \nu$, where U_τ is the friction velocity, δ is the boundary layer thickness, and ν is the kinematic viscosity of air.

Figure 1 shows the experimental setup. The measurement array consists of a single hotwire attached to a moving traverse, two spanwise arrays of flush-mounted skin-friction sensors, and a rectangular jet. The two spanwise arrays are located 2δ apart in the streamwise direction, with the jet positioned in between the two arrays. Each of the spanwise array consists of 9 skin-friction sensors, covering a spanwise domain of 0.64δ , with a spanwise resolution $\Delta y = 0.026$ m or 0.08δ . These sensors are Dantec 55R47 glue-on type sensors and are operated in constant-temperature mode using AA labs AN1003 anemometer with overheat ratio (OHR) set to 1.05.

The hotwire probe is mounted with its sensing element 550 mm upstream of the leading edge of the traversing sting. To minimize flow disturbance, the sting has an airfoil profile resembling NACA0016 with chord length of 180 mm. The hotwire prong has a spacing of 1.25 mm with 2.5-micron-diameter Wollaston platinum wire soldered between the prongs. Its etched length is 0.5 mm, keeping length to diameter ratio of 200, in accordance to the recommendations of Ligrani and Bradshaw (1987). It is operated with a OHR of 1.8 using an in-house-developed Melbourne University Constant Temperature Anemometer (MUCTA). The

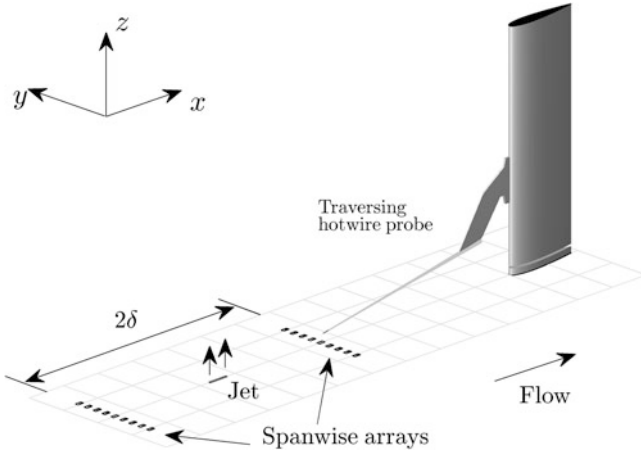


Fig. 1 Schematic of experimental setup

dimensions, specifications, and relative positions of the skin-friction sensors in both the arrays are similar to the configuration used by Hutchins et al. (2011). Throughout this chapter, x , y , and z represent the streamwise, spanwise, and wall-normal directions with u , v , and w denoting the respective fluctuating velocity components.

The hotwire is calibrated in situ against a Pitot-static tube at 12 different free-stream velocities ranging from 0 to 25 m/s, while the hot-film sensors are calibrated using the friction velocity values at the above velocities obtained from previously reported results at the same location. Any errors in hot-film calibration will have only minimal effect on the analysis presented here since these sensors are merely used as low/high-skin-friction detection sensors.

3 Off-line Control Scheme

As a first step toward understanding the interactions of jet with the large-scale structures, an off-line control strategy is investigated. In these experiments, no real-time active controller is implemented, but the jet is periodically fired with fixed parameters, and during post-processing, the ‘control’ strategy is emulated in a conditional sense. The jet velocity is set at 10 m/s and is actuated for 0.1 s in a duty cycle of 0.4 s, while all the skin-friction sensors and hotwire are simultaneously sampled. In the post-processing stage, selective parts of the signal from the sensors are collected, where the jet has truly targeted a large-scale structure, as illustrated in Fig. 2. In this figure, the three signals, filtered upstream skin-friction signal, the jet, and the hotwire are shown with appropriate time shifts. Here, the length of hotwire signal enclosed by two dotted vertical lines is an example of

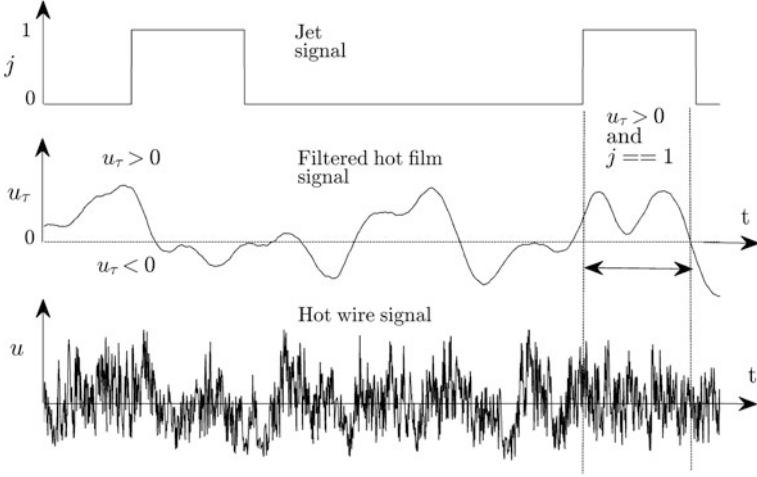


Fig. 2 Off-line-simulated control scheme

large-scale high-skin-friction signal ($u_\tau > 0$) that is being targeted by the jet, and the effect is studied using the downstream hotwire signal.

4 Conditional Events

The interaction of the jet with the large-scale skin-friction fluctuations and the streamwise velocity fluctuations can be studied by computing conditional averages from the skin-friction sensors and the hotwire probe conditioned on the passage of a high-skin-friction event and also targeted by the jet after a certain time delay. The signal from the upstream wall shear-stress sensor is used to detect the structures convecting above it. This signal is filtered using a low-pass Gaussian filter of length 0.5δ to get a signature of the large-scale skin-friction events. Using this large-scale signal, a high-skin-friction event is identified when the fluctuating friction velocity is greater than zero, and conversely, a value below zero indicates a low-skin-friction event. All the sensors including the control signal of the jet are simultaneously sampled. The conditional average is defined as

$$u|_{\text{hj}}(\Delta t, \Delta y, z) = \langle u(t, y, z) | u_\tau(t - \Delta t, y - \Delta y) > 0 \& j(t - \Delta t + \Delta T, y - \Delta y) = 1 \rangle \quad (1)$$

is a function of the wall-normal, spanwise, and temporal separation. Using Taylor's hypothesis with $x = -U_c t$, it can be converted to a function of all three spatial coordinates

$$u|_{\text{hj}}(\Delta x, \Delta y, z) = \langle u(x, y, z) | u_\tau(x - \Delta x, y - \Delta y) > 0 \& j(x - \Delta x + \Delta X, y - \Delta y) = 1 \rangle \quad (2)$$

In these equations, u is the streamwise velocity fluctuation and u_τ is the friction velocity fluctuation, j is the binary control signal of the jet, ΔX is the physical separation between the jet and the downstream array, and U_c is the convection velocity. In all the figures presented in this paper, $x = 0$ represents the streamwise location of upstream skin-friction sensor array, $x = 1 \delta$ is the location of the jet, and $x = 2 \delta$ is the location of the hotwire probe and the downstream array of sensors.

4.1 Two-Dimensional Conditional View

Figure 3a shows the two-dimensional skin-friction fluctuations from the downstream array of hot-film sensors when conditioned on a positive skin-friction fluctuation on upstream sensor 5. A region of elongated positive skin-friction fluctuations is flanked on both sides by anti-correlated behavior with a spanwise separation of $0.7 - 0.8 \delta$ between two positively correlated regions. Such behavior has been previously reported by Hutchins and Marusic (2007a), but in the current study, it is also possible to look at such a conditional high-skin-friction event when targeted by a jet, which is shown in Fig. 3b. It is evident that the jet has modified the elongated positive region along the line of symmetry at $\Delta y = 0$, but appears to have enhanced the positive skin-friction fluctuations on both sides of the centerline. However, merely analyzing the effect of the jet on the skin-friction footprint can be misleading. To resolve this, it is useful to look at the three-dimensional conditional view of the velocity fluctuations, which will be discussed in the following section.

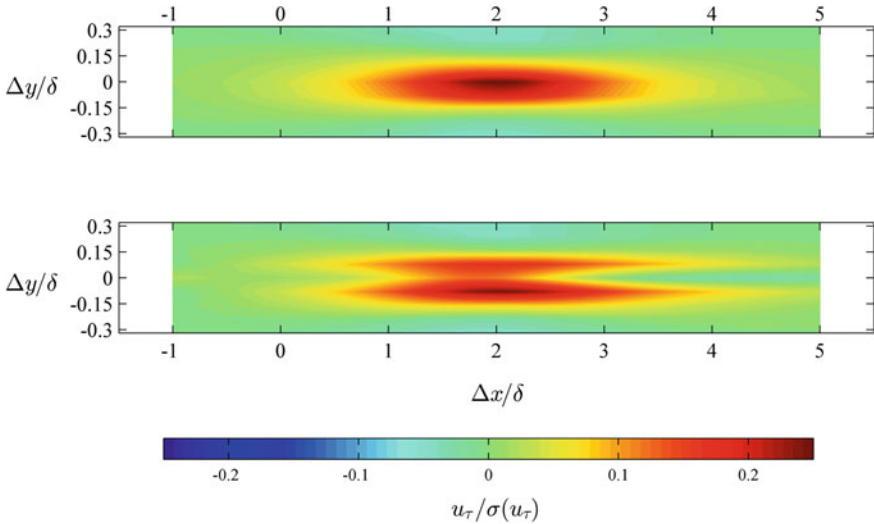


Fig. 3 Isocontours of skin-friction fluctuations conditionally averaged on a high-skin-friction event (a) unmodified flow (b) simulated off-line control scheme

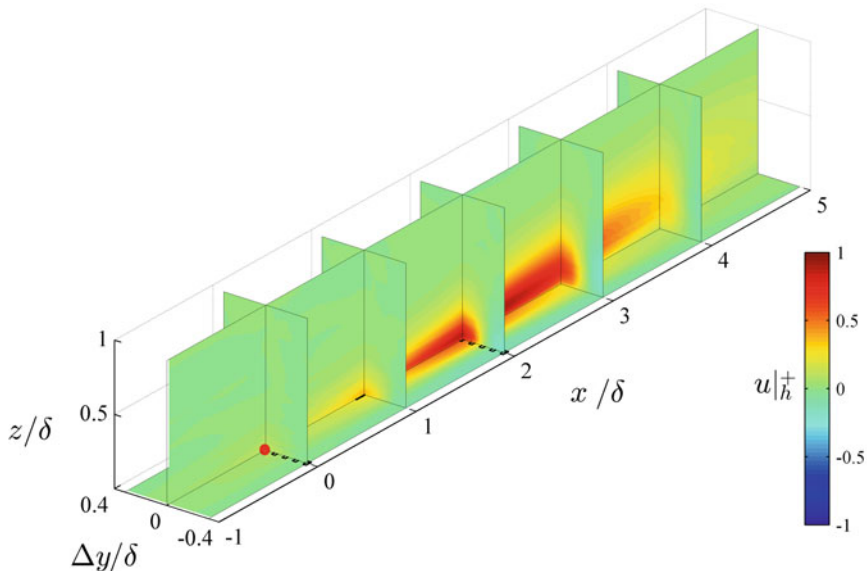


Fig. 4 Isocontours of streamwise velocity fluctuations conditionally averaged on a high-skin-friction event

4.2 Three-Dimensional Conditional View

Besides looking at the skin-friction fluctuations at the wall, the simultaneous time-series measurements from hotwire and skin-friction sensors allowed us to compute a conditionally averaged view of velocity fluctuations that occur in two cases: (1) unmodified and (2) modified high-skin-friction events. To build a three-dimensional conditional view, several experiments are conducted by positioning the jet in different spanwise locations in line with one of the nine skin-friction sensors. The data from these experiments have been used to compute the conditional averages in different spanwise planes according to Eq. 2, and by putting together all the data in such planes, a three-dimensional conditional view was built.

Figure 4 shows the isocontours of streamwise velocity fluctuations during an unmodified high-skin-friction event on upstream sensor 5 (shown as red dot), in different x - y , y - z , and y - z planes, $x/\delta = 0, 1, \dots, 4$, $\Delta y/\delta = 0$, and $z/\delta = 10^{-4}$. The figure reveals an inclined, forward-leaning, high-speed structure extending over 3δ in the streamwise direction. Such an observation is totally consistent with recent studies in the literature, see for example Hutchins et al. (2011). Flanking the high-speed region in the center, there are two low-speed regions in the spanwise

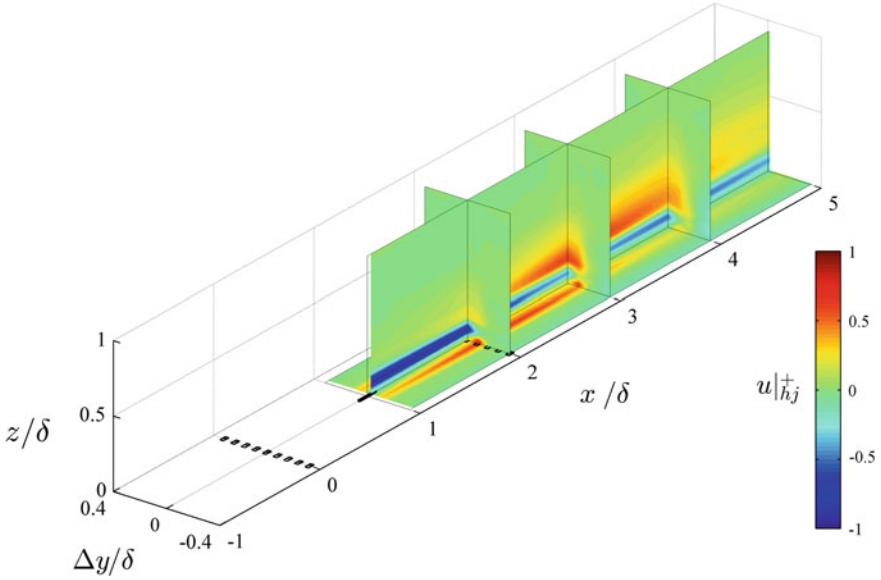


Fig. 5 Isocontours of streamwise velocity fluctuations conditionally averaged on a high-skin-friction event and targeted by a jet

direction, separated by a distance of $0.7 - 0.8 \delta$, similar to the result observed in the conditional wall shear-stress fluctuations in Fig. 3.

The motivation in this study is to modify the conditional high-skin-friction events using a wall-normal jet. As explained previously, a control scheme is simulated in the post-processing stage, and the results from the analysis are presented in Figs. 5 and 6. Note that in these figures, only the data behind the jet's location ($x/\delta = 1$) are presented as Taylor's hypothesis is no longer valid upstream of the jet's location. Figure 5 shows that the jet has penetrated to a depth of 0.1δ into the boundary layer, reducing the intensity of velocity fluctuations in the central plane corresponding to $\Delta y = 0$. However, its effect seems to be very localized with signs of increased skin-friction fluctuations on both sides.

To illustrate this better, the same result is plotted in Fig. 6 in three cross-planes at $x/\delta = 2, 3, 4$. Another inference that can be made here is that the jet has created a pair of streamwise roll modes, represented as circular arrows in the figure. Although this study only measured the streamwise component of the modified flow, the result seems to point toward this case. However, the scale of such roll modes is considerably small compared to the indicative naturally occurring roll modes, which are of the size 0.5δ , as reported by Talluru et al. (2012).

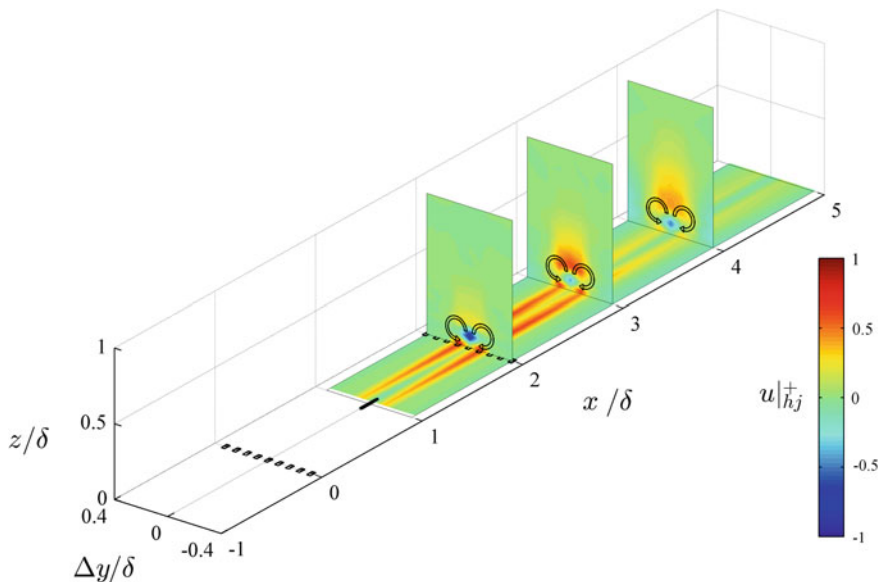


Fig. 6 Isocontours of streamwise velocity fluctuations conditionally averaged on a high-skin-friction event shown in three streamwise cross-planes

5 Conclusions

Two spanwise arrays of glue-on hot-film sensors along with a wall-normal jet and a traversing hotwire probe are used to study the interaction of a jet with the large-scale structures that populate the logarithmic region of a turbulent boundary layer. Initial experiments were conducted with a periodic actuation of the jet, and the effects are studied in a conditional sense to emulate the behavior of an effective large-scale, real-time control scheme.

The conditional results show that the jet is able to generate a low-speed region along the symmetric plane, affecting the large-scale high-speed structure. However, it also appears to have increased the positive velocity and skin-friction fluctuations on both sides of the symmetric plane. An initial inference is made here; the jet actuation has induced streamwise counter-rotating roll modes into the flow; however, this observation has to be further justified by looking at the spanwise and wall-normal components of the velocity. Finally, the effect produced by the jet seems to be too localized and small compared to the scale of the large-scale high-skin-friction events and their associated streamwise roll modes. As a more general concluding statement, these results show prospects of using a wall-normal jet to target the large-scale control schemes when implemented at the correct scale.

References

- Adrian RJ (2007) Hairpin vortex organization in wall turbulence. *Phys Fluids* 19:041301
- Beresh S, Henfling JF, Spillers RS, Pruet B (2011) Improved measurements of large-scale coherent structures in the wall pressure field beneath a supersonic turbulent boundary layer. In: 41st AIAA fluid dynamics conference and exhibit
- Chung D, McKeon BJ (2010) Large-eddy simulation of large-scale structures in long channel flow. *J Fluid Mech* 661:341–364
- Dennis DJC, Nickels TB (2011) Experimental measurement of large-scale three-dimensional structures in a turbulent boundary layer. Part 1: vortex packets. *J Fluid Mech* 673:180–217
- Guala M, Metzger M, McKeon BJ (2011) Interactions across the turbulent boundary layer at high Reynolds number. *J Fluid Mech* 666:573–604
- Haven BA, Kurosaka M (1997) Kidney and anti-kidney vortices in cross flow jets. *J Fluid Mech* 352:27–64
- Hutchins N, Monty JP, Ganapathisubramani B, Ng HCH, Marusic I (2011) Three dimensional conditional structure of a high-Reynolds-number turbulent boundary layer. *J Fluid Mech* 673: 255–285
- Hutchins N, Marusic I (2007a) Evidence of very long meandering features in the logarithmic region of turbulent boundary layers. *J Fluid Mech* 579:1–28
- Hutchins N, Marusic I (2007b) Large-scale influences in near-wall turbulence. *Phil Trans R Soc A* 365:647–664
- Hutchins N, Chauhan K, Marusic I, Monty J, Klewicki J (2012) Towards reconciling the large-scale structure of turbulent boundary layers in the atmosphere and laboratory. *Bound-Layer Meteorol* 1–34
- Kim KC, Adrian RJ (1999) Very large-scale motion in the outer layer. *Phys Fluids* 11(2):417–422
- Kulandaivelu V (2012) Evolution of zero pressure gradient turbulent boundary layers from different initial conditions. PhD Thesis, The University of Melbourne, Australia, 2012
- Ligrani PM, Bradshaw P (1987) Spatial resolution and measurement of turbulence in the viscous sublayer using subminiature hot-wire probes. *Exp Fluids* 5:407–417
- Marusic I, Mathis R, Hutchins N (2010) Predictive model for wall-bounded turbulent flow. *Science* 329(5988):193–196
- Mathis R, Hutchins N, Marusic I (2009) Large-scale amplitude modulation of the small-scale structures in turbulent boundary layers. *J Fluid Mech* 628:311–337
- Savill AM, Mumford JC (1988) Manipulation of turbulent boundary layers by outer-layer devices: skin-friction and flow-visualization. *J Fluid Mech* 191:389–418
- Talluru KM, Morrill-Winter C, Ebner R, Hutchins N, Klewicki J, Marusic I (2012) Three dimensional conditional structure of large-scale structures in a high Reynolds number turbulent boundary layer. In: Proceedings of 18th Australasian Fluid Mechanics Conference, Launceston, Australia
- Tomkins CD, Adrian RJ (2003) Spanwise structure and scale growth in turbulent boundary layers. *J Fluid Mech* 490:37–74